ResearchGate

See discussions, stats, and author profiles for this publication at: https://www.researchgate.net/publication/274380807

Overcoming Coulombic Traps: Geometry and Electronic Characterizations of Light-Induced Separated Spins at the Bulk Heterojunction Interface

ARTICLE *in* JOURNAL OF PHYSICAL CHEMISTRY LETTERS · DECEMBER 2014

Impact Factor: 7.46 · DOI: 10.1021/jz5023202

CITATIONS
4

READS
32

2 AUTHORS, INCLUDING:

Yasuhiro Kobori
Kobe University
48 PUBLICATIONS **841** CITATIONS

SEE PROFILE

Available from: Yasuhiro Kobori
Retrieved on: 30 January 2016

THE JOURNAL OF PHYSICAL CHEMISTRY Letters

Perspective

pubs.acs.org/JPCL

Overcoming Coulombic Traps: Geometry and Electronic Characterizations of Light-Induced Separated Spins at the Bulk Heterojunction Interface

Yasuhiro Kobori*[,§,†] and Taku Miura[§]

[§]Department of Chemistry, Graduate School of Science, Kobe University, 1-1 Rokkoudai-cho, Nada-ku, Kobe 657-8501, Japan

[†]PRESTO, Japan Science and Technology Agency, 4-1-8 Honcho, Kawaguchi-shi, Saitama 332-0012, Japan

ABSTRACT: Recent progress is overviewed on experimental elucidations of fundamental molecular functions of the light−energy conversions by the photoactive layers of the organic photovoltaic (OPV) cells by means of the time-resolved electron paramagnetic resonance spectroscopy. Positions and orientations of the unpaired electrons and electronic coupling matrix elements are clarified in photoinduced, primary charge-separated (CS) states. Connections between the molecular geometries and the electronic couplings have been characterized for the initial CS states to elucidate how the structure, orbital delocalization, and molecular libration play roles on exothermic carrier dissociation via a vibrationally relaxed charge-transfer complex with prevention of the energy-wasting charge recombination. Superior functions to biological molecules are presented for the efficient photocurrent generations induced by orbital delocalization and by shallow trap depths at polymer-stacking domains. The above structural and electronic characteristics of the primary electron−hole pairs are essential to evaluations, designs, and developments of the efficient solar cells using organic molecules.

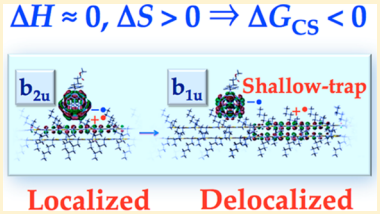

Organic photovoltaic (OPV)[1] devices have recently attracted much attention as the next-generation thin-film solar cells that can be low-cost, flexible, and light compared to the conventional silicon solar cells.[2] The spin-coating method from mixed solutions consisting of conjugate polymers as the electron donors (D) and fullerene derivatives as the acceptors (A) are employed to produce the solid photoactive layer of the OPV cells.[1] Recent progress in organic materials[3,4] and in device structures[5] have enabled remarkably efficient OPV cells as high as 12% in light−energy conversion efficiency, which is however still lower than 25% in the silicon solar cells. In the organic photoactive layers, it is well-known that the molecules tend to be self-organized to form phase segregation by the polymers and by the fullerene derivatives to generate the bulk heterojunction (BHJ)[1,2] by the domain interfaces, as shown in Figure 1. The BHJ thin-films[6] composed of poly(3-alkylthiophene) (P3AT) as the D and [6,6]-C_{61}-butyric acid methyl ester ($PC_{60}BM$) as the A in Figure 1 have been regarded as a standard and representative material of the photoactive layer in the OPV devices.

The polymer−fullerene phase segregation is in the range of 5−10 nm, which is the excition diffusion length.[6] This small domain size thus can contribute to the efficient photoinduced charge-transfer (CT) reaction at the polymer−fullerene interfaces.

Extensive studies have been performed to investigate the physical and photochemical properties of the OPV-related materials. Saeki et al.[7] have found a good correlation between the power conversion efficiencies (PCEs) and the photoinduced transient conductivity signals of the several blend films as measured by the time-resolved microwave photoconductivity method, indicating that the light-driven, initial electron and hole motilities are keys to the OPV performance. The ultrafast photoinduced charge injection dynamics has been clarified by the light excitations of poly(3-hexylthiophene-2,5-diyl) (P3HT) domains in the P3HT/PCBM blend films.[6,8−11] Recent studies have demonstrated that the photoinduced contact CT states are initially generated at the D/A domain interfaces and play significant roles on the photocurrent generations in the P3AT/PCBM blends.[10,12−17] However, femtosecond transient spectroscopy has indicated the existence of higher-energy, faster dissociating pathways at the D/A interfaces for the other blend materials.[18] Very recently, Vandewal et al.[15] demonstrated for the several polymer/PCBM solar cells that the internal quantum efficiency (IQE) is essentially independent of the excitation energy of the lights; even if the low-energy CT absorption band is excited, the IQE is higher than 90% for some blend films, giving rise to very high OPV performances. The electrons and holes need to escape from the Coulomb attraction, whose energy is supposed to be several hundreds of meV in the CT state.

To elucidate why and how the photocarriers escape from the CT binding, it is important to directly observe not only the separation distances between the electron and the hole but also the relative molecular positions and orientations of the charged species just after the interfacial charge conductions in Figure 1. As for such separated electron−hole pairs, the electronic coupling matrix elements (V_{CR}) are key interactions to understand how the energy-wasting charge-recombination (CR) processes are inhibited. Connection between the geometry and the V_{CR} in the charge-separated (CS) state will also lead to

Received: November 1, 2014
Accepted: December 12, 2014
Published: December 12, 2014

 © 2014 American Chemical Society dx.doi.org/10.1021/jz5023202 | *J. Phys. Chem. Lett.* 2015, 6, 113−123

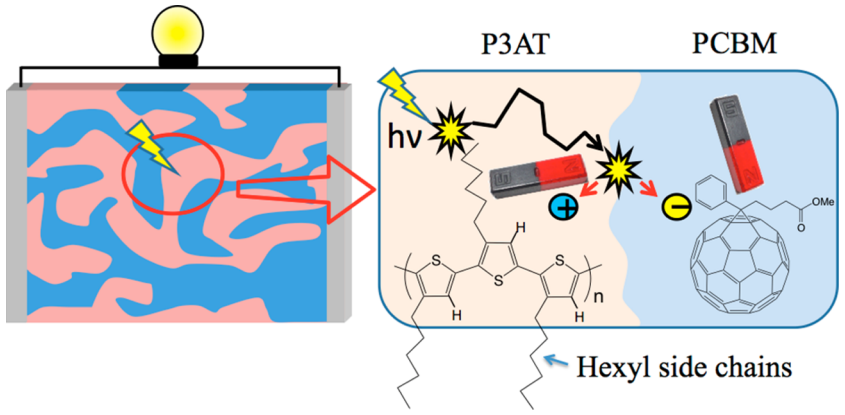

Figure 1. Schematic view of the BHJ structure by the domains in the photoactive layer of the OPV cell. The separated electron−hole pairs are generated via the contact CT states at the polymer (P3AT)/fullerene ($PC_{60}BM$) domain interfaces.

unveiling (1) the initial photoconduction pathways by the molecular orbitals and (2) the electronic conduction characteristics relating to the trap depth at the D/A domain interface. The molecular motion in the organic semiconductors is another key to the efficient dissociation. The molecular libration in the blend should enhance the entropy of the dissociated CS state as compared to that of the bound CT state, as emphasized by Clarke and Durrant.[19]

The time-resolved electron paramagnetic resonance (TREPR) spectroscopy is very powerful to clarify the above-mentioned characters of the intermediate species.[20−29] Figure 2 shows a model structure of a pair of unpaired orbitals in the CS state for the complex by the D and A molecules at the P3HT/$PC_{60}BM$ domain interface. If the photoinduced CS state of $P3HT^{+\bullet}$···$PC_{60}BM^{-\bullet}$ is immediately generated by nanosecond pulsed laser irradiations as in Figure 1, because these separated charges have the magnetic moments by the electron spins, the external magnetic field (B_0) by the EPR magnet will induce the Zeeman interactions (= $g\beta B_0$, where g and β denote the g factor and the Bohr magneton, respectively)[30] in Figure 2. If the two electron spins are significantly separated and are not magnetically coupled, the EPR transitions will take place at $B_{res} = h\nu/(g\beta)$, where ν is the microwave frequency, resulting in the two EPR lines separated by the difference in the g factors between $P3HT^{+\bullet}$ and $PC_{60}BM^{-\bullet}$.[3,31−33] The electron−nuclear hyperfine interaction (HFI) in the radical is determined by the nuclear spin quantum number (I = 1/2 or −1/2 in the case of the protons, as shown in the polymer backbone in Figure 1) of the interacting nuclear spins in Figure 2 and provides additional magnetic field from the nuclear spins to the electron spins, resulting in some broader EPR lines. If the two electron spins are magnetically coupled by the electron spin−spin dipolar interaction (D), one charge will be a source of a magnetic field to the other charge by the magnetic moment.[22] Thus, the EPR spectrum can become significantly broader when the electron−hole separation is smaller.[3,22,34] In the quantum mechanical description, the above Zeeman, HFI, and D interactions will contribute to the triplet spin sublevels in the CS state as formulated by the Schrödinger equation.[30] The Zeeman, the HF, and the D couplings all depend upon the direction ($\boldsymbol{\Omega}$) of B_0 with respect to a reference axis system in Figure 2. As an example, the D is proportional to $(1 - 3\cos^2\theta_D)/r_{CC}^3$, where θ_D and r_{CC} are an angle between the interspin vector ($\boldsymbol{d}$) and $\boldsymbol{\Omega}$ and the interspin separation, respectively.[30] Thus, the spin energy levels of the CS state are affected by a combination of the relative molecular position (as determined by the direction of $\boldsymbol{d}$) and of the orientation of the red axis system (g_X, g_Y, g_Z) with respect to the blue axis system (g_x, g_y, g_z), which are given by the Euler angles.[28,35,36] Because the TREPR spectrum reflects the microwave transitions between the spin sublevels, quantum mechanical analyses of the EPR spectra will lead to determinations of the geometry of the transient CS states.[25] Moreover, the isotropic spin−spin exchange coupling ($2J$) is generated by the overlap between the two unpaired orbitals in Figure 2, producing the singlet (S)−triplet energy splitting in the CS states. According to the spin correlated radical pair (SCRP) mechanism,[21,23,33,36] the combination of the HFI and the J determines the state mixing between the S and a triplet sublevel of the T_0 state in the presence of B_0 and thus affects the EPR transitions. The $2J$ in the separated CS states has been known to be dominated by the configuration interaction[36−41] in accordance with the Marcus electron-transfer (ET) theory and is approximated by $|2J_i| = |V_{CR,i}|^2/|\Delta E_{CR,i}|$, where $\Delta E_{CR,i}$ is the vertical energy gap for the CR to the state i. Therefore, from the TREPR spectrum, one is able to characterize the V_{CR} together with the molecular geometries in the CS state.[34,42−44]

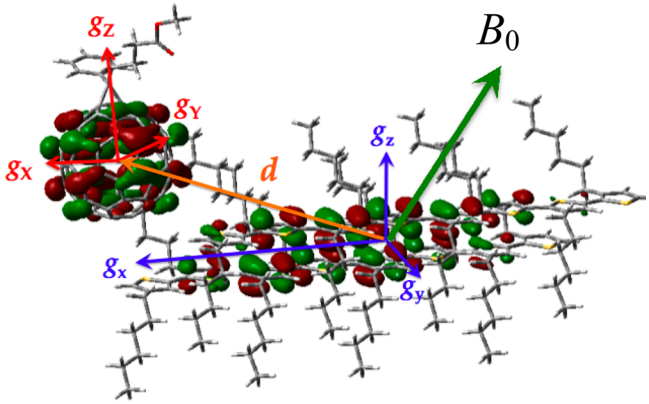

Figure 2. Relations between the molecular geometries and the anisotropic magnetic interactions represented by the principal axis systems of the g tenors and by the electron spin−spin dipolar interaction ($\boldsymbol{d}$) depicted on the unpaired orbitals of a photoinduced CS state.

Numerous experimental and theoretical studies have been conducted to clarify the carrier dissociation mechanism in the organic semiconductors.[3,6,10,13−16,18,33,34,45−49] However, only a few studies[34,44] have experimentally elucidated the (1) CS geometries, (2) electronic characters by the unpaired orbitals,

dx.doi.org/10.1021/jz5023202 | J. Phys. Chem. Lett. 2015, 6, 113−123

and (3) libration motion or distribution contributing to the carrier dissociations at the BHJ domain interface. In this Perspective, recent progresses are overviewed on the experimental elucidations of the fundamental light−enegy conversion functions on the initially gerarated interfacial electron−hole pairs at the photoactive layers in Figure 1.

Determinations of Geometries of the Interfacial Photoinduced CS States. Highly quick charge dissociation dynamics has been known after the interfacial photoinduced ET process in the blend materials.[9,14,16] To characterize the CS state geometry, the electronic coupling, and the molecular motion at the domain interface by the TREPR, the carrier mobilites are required to be frozen with respect to the mobilities under the conditions that the OPV devices work at room temperature. The microwave photoconductance measurements[9] have revealed that the carrier mobilities become much smaller at cryogenic temperature. One recent low-temperature transient absorption study[49] has demonstrated that the positions of the initially separated electron−hole pairs are frozen at a few nanometer intercarrier distances at the D/A interfaces for several polymer/PCBM blend films. Furthermore, a first-order decay of the microwave photoconductance is reported at cryogenic temperatures and was explained by the predominance of the geminate CR process of the electron−hole pairs.[9] Thus, it is highly expected that one is able to characterize the geometries of the separated electron−hole pairs in the BHJ materials by using the TREPR.

Figure 3 shows examples of the TREPR data obtained by the nanosecond 532 nm laser irradiations at T = 77 K of spin-coated

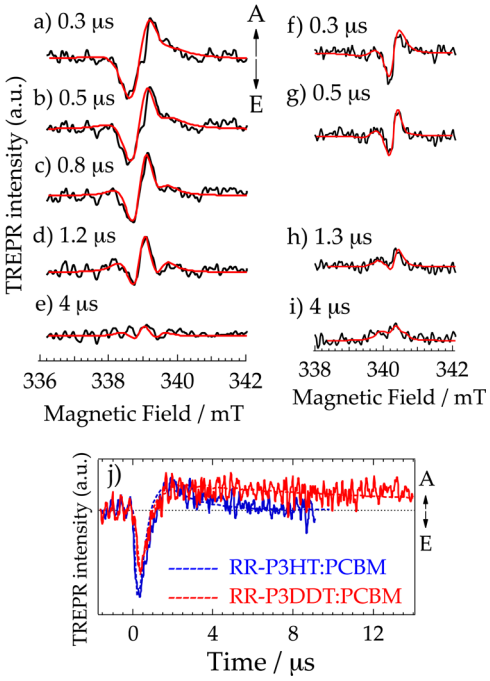

Figure 3. TREPR spectra of the as-spun films of RR-P3HT/$PC_{60}BM$ (a−e) and of RR-P3DDT/$PC_{60}BM$ (f−i) blend films obtained at several delay times after the 532 nm laser excitations at T = 77 K. (j) Time evolutions in the transient EPR of the initial emissive signals for the RR-P3HT/$PC_{60}BM$ (blue line at B_0 = 338.6 mT) and for the RR-P3DDT/$PC_{60}BM$ (red line at B_0 = 340.2 mT).

thin films (spun at 3000 rpm for 30 s on a glass substrate resulting in a thickness of ∼20 nm).[44] To enhance the time resolution, we did not employ the standard phase-sensitive detection by the field modulation. We have directly monitored a preamplified TREPR signal using a digital oscilloscope. Note that in the TREPR measurements, highly long-lived stable species accumulated by the light irradiations are filtered by the preamplifier and are thus not detectable.[34] At the left, TREPR spectra are shown for the as-spun film fabricated from the regioregular (RR)-P3HT/$PC_{60}BM$ (1:1 by weight) dissolved in 1,2-dichrolobenzene.

The right spectra are from the 1:1 blend of regioregular poly(3-dodecylthiophene-2,5-diyl) (RR-P3DDT)/$PC_{60}BM$ to investigate the effect of the increased alkyl side chain on the geometry and on the electronic coupling of the transient CS state in the RR-P3AT/PCBM system. It is noted here that the ground-state absorption spectrum of the RR-P3DDT/PCBM film exhibits the exciton band by the crystalline phase of the P3AT domain, which is very similar to the band by the RR-P3HT/PCBM film, as reported in the Supporting Information of our previous study.[44] The positive signal denoted by A is the TREPR intensity (transverse magnetization) by the microwave absorption, while the negative direction of E is the emission in Figure 3. The shifts of the resonant fields (B_{res}) in the right spectra with respect to the left spectra are caused by the difference in the applied microwave frequencies (ν). The signal field positions in Figure 3 were consistent with the resonance positions of the dissociated polarons of $P3AT^{+\bullet}$ and $PC_{60}BM^{-\bullet}$ obtained by the steady-state EPR measurements[31] using the standard phase-sensitive detections. The coexistence of the A and E polarizations is explained by the initial population in the T_0 of the CS state. This T_0 production is due to the coherent S−T_0 interconversions by the HFI and by the g value difference between $P3AT^{+\bullet}$ and $PC_{60}BM^{-\bullet}$ after the singlet CS process under the weak J and D couplings in the SCRP, producing the absorptive $T_0 \rightarrow T_+$ and the emissive $T_0 \rightarrow T_-$ transition moments, as shown in Figure 4. Thus, the initial A/E pattern

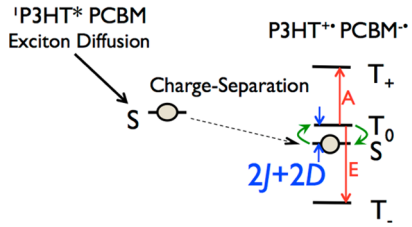

Figure 4. Schematic representation of the EPR transitions after the interfacial singlet CS process followed by the exciton diffusion in the P3HT region. The coherent S−T_0 interconversion (as denoted by green arrows) produces both the absorptive (A) and emissive (E) EPR transition probabilities. The resonant field positions and intensities are however affected by the S−T_0 mixing determined by the HFI, the J and the D and thus are dependent on the CS geometry and of the J in Figure 2. The effects of the spin relaxations and the CR kinetics are not depicted in this figure but are required to be taken into account to fully reproduce the time developments of the EPR spectra in Figure 3

(Figure 3a) and the E/A/E/A (Figure 3f) reflect the microwave transition probabilities between the triplet sublevels,[34] those of which are determined by the geometry and the electronic coupling in the CS state. One can see that the spectrum shapes and amplitudes are changed by the delay times in Figure 3. Combinations of the spin relaxations and the spin-selective CR kinetics with frozen geometries and electronic couplings explained these delay time dependences, as detailed in our previous studies.[34,44] From Figure 3a and f, by replacing the hexyl side chains with the dodecyl ones in the polyalkylthiophene, the spectrum widths become much smaller compared with the widths in Figure 3a, denoting that the D coupling is significantly

dx.doi.org/10.1021/jz5023202 | J. Phys. Chem. Lett. 2015, 6, 113−123

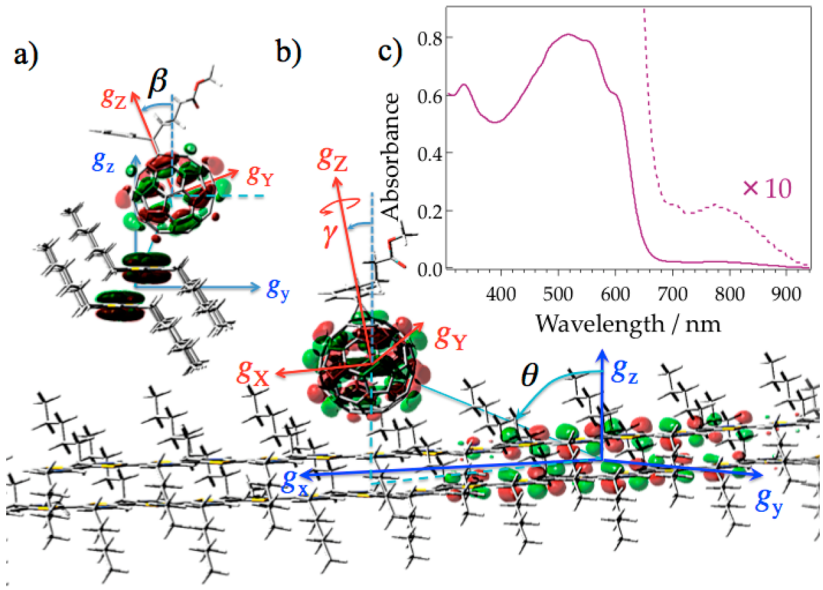

Figure 5. (a,b) One of the geometries of the interfacial photoinduced CS state to reproduce the TREPR spectra (left in Figure 3) for the as-spun film of the RR-P3HT/$PC_{60}BM$ blend at $T = 77$ K. (a) The view of the CS state from the g_X axis in the $P3AT^{+\bullet}$. (b) The entire view of the CS state, representing that the hole initially escapes from the electron in $PC_{60}BM^{-\bullet}$ with $\theta = 50°$ to the center-to-center separation of ∼15 Å. The γ angle can be treated to be arbitrary because of $g_X \approx g_Y$.[34] (c) UV−vis absorption spectrum of the blend films of the 1:1 RR-P3HT/$PC_{60}BM$, showing a strong CT absorption by the stacked P3HT/$PC_{60}BM$ complex at around 770 nm.

weakened (from $D = -0.63$ to -0.20 mT)[44] in the CS state. Evidently, the decay of the thermal equilibrium absorption (red line) in Figure 3j is much slower in the P3DDT/$PC_{60}BM$ system than that in the P3HT/$PC_{60}BM$ system (blue line), indicating that the CR process is highly suppressed by the more separated electron spins. These results are explained by the initial generation of the distant CS state by the electron−hole dissociation in the P3AT/$PC_{60}BM$.

There are several reports accounting for the efficient photocarrier dissociations by the electron delocalization in the PCBM clusters at elevated temperatures of $T > 170$ K, as reported in ref 46. At 77 K, however, the electron mobility of $PCBM^{-\bullet}$ is reported to be several orders of magnitude smaller than the hole mobility of $P3HT^{+\bullet}$ in the P3HT/PCBM blend film from the microwave photoconductance measurements in ref 9. Our previous TREPR study[34] showed that the CS distance is significantly smaller (∼1 nm) in the regiorandom-P3HT/PCBM system than the distance (∼2 nm) in the RR-P3HT/PCBM system at 77 K. Such a polymer effect clearly denoted that the photoinduced charge dissociation is dominated by the hole delocalization by the polymer molecules at 77 K.[34] Additionally, low-temperature EPR observations of the anisotropy[31] in the g factor of $PCBM^{-\bullet}$ demonstrate that the electron spin is not delocalized in the PCBM cluster but localized in one PCBM in the blend films.[34] Because the PCBM cluster is composed of several PCBM molecules that are differently oriented, the g anisotropy should be disappeared if the unpaired electron is delocalized. At the 77 K condition, one can thus consider that the electron is trapped in one PCBM molecule and that the $PCBM^{-\bullet}$ position is frozen after the initial electron injection from the polymer to the PCBM domain.

To clarify the electron−hole dissociation mechanism and the electronic property of the photoinduced CS states, the nanostructures and the $2J$ were obtained by the analyses of the TREPR data (the red lines in the TREPR spectra and the red dashed lines in the time traces in Figure 3) on the basis of the stochastic-Liouville equation (SLE) by which the time-dependent quantum mechanical phenomena in the density matrix ($\boldsymbol{\rho}$) of the singlet−triplet system are solved in the rotating frame on the basis spin functions of $|T_+\rangle = |\alpha\alpha\rangle$, $|T_0\rangle = |\alpha\beta + \beta\alpha\rangle/\sqrt{2}$, $|T_-\rangle = |\beta\beta\rangle$ for the triplet CS state and of $|S\rangle = |\alpha\beta - \beta\alpha\rangle/\sqrt{2}$ for the singlet CS state in Figure 4.[34,44,50] The effects of the spin relaxations (the spin−lattice relaxation time of T_1, the transverse relaxation times T_2, and the relaxation time of T_{23} by the S−T_0 dephasing[51]) and the CR kinetics were taken into account in the SLE.[34,44] Theoretical details concerning how one can calculate the time evolutions of the transverse magnetizations have been reported in the Suppoting Information files in our previous studies.[34,44] Also, detailed discussions how the angle parameters, the dipolar coupling, and the electronic coupling affect the computation results have been described in ref 34.

The Euler angles of the principal g axis system of $PC_{60}BM^{-\bullet}$ with respect to the g-axis system in $P3AT^{+\bullet}$ are defined by (α, β, γ) with the x-convention.[34] The directions of the dipolar principal axis between $P3AT^{+\bullet}$ and $PC_{60}BM^{-\bullet}$ are defined by the polar angles θ and ϕ with respect to the principal g tensor axes in $P3AT^{+\bullet}$, as shown in Figure 5b.[31,52] Because $g_X \approx g_Y$ in $PC_{60}BM^{-\bullet}$, effects of the γ angles cannot be exactly distinguished by the SLE analysis.[34] In fact, because the heterogeneous rotational angles of $PC_{60}BM^{-\bullet}$ shall be allowed along the g_Z axis, the parameter of the γ can be treated as arbitrary in Figure 5b. Although the TREPR spectrum is highly sensitive to the CS geometry as determined by $(\theta, \phi, \alpha, \beta)$, it should however be noted that there are several combinations of the four angle parameters to reproduce the TREPR spectra, as reported in the previous analysis.[34] Nevertheless, several angle sets will generate highly hindered RR-P3AT/$PC_{60}BM$ complexes caused by the alkyl side chains and by the substituents in $PC_{60}BM$, those of which are thus excluded. Also, one is able to discuss the validities of the structural determinations of the CS state with the assistance of several other reported spectroscopic and structural observations, as detailed in the following.

dx.doi.org/10.1021/jz5023202 | J. Phys. Chem. Lett. 2015, 6, 113−123

One of the nanostructures of the CS states to reproduce the TREPR data is depicted for the as-spun RR-P3HT/$PC_{60}BM$ film in Figure 5a and b. The structure of $P3AT^{+\bullet}$ in the P3AT region is based upon a recent electron diffraction analysis that has revealed a tilted packing structure[53,54] with the short $\pi-\pi$ stacking of a 3.4 Å interplanar distance in the crystalline P3HT. This $\pi-\pi$ stacking is coincident with the UV−vis absorption spectrum of the blend films of the 1:1 RR-P3HT/$PC_{60}BM$, showing dominant strong vibrational absorption bands at around 530 nm in Figure 5c that are characteristics of the crystalline phase by the RR-P3HT molecules.[55] The interchain delocalized hole distribution is consistent with the dimer polaron model,[56] which explains the absorption spectra of the polarons reported in the crystalline RR-P3HT phase. $\beta = \pm 18-20°$ was obtained as a tilt angle between the out-of-plane direction of P3HT and the top (g_Z) direction of the $PC_{60}BM^{-\bullet}$ molecule. $\beta = \pm 18-20°$ implies that the hexagonal or pentagonal aromatic ring at the $PC_{60}BM$ bottom faces the aromatic plane of P3HT, giving rise to the strong π-stacking interactions with the aromatic P3HT plane, as shown in Figure 5a. This is well compatible with the CT transition band[12,57] in Figure 5c at around 770 nm and with the reported model structures of the P3HT/$PC_{60}BM$ CT complexes.[8,10,12] These aromatic stacking situations in Figure 5a explain the efficient electron injection dynamics from ^{1}P3HT* to $PC_{60}BM$ by the contact CT character, as described above. In Figure 5a, the height (h) is found to be $h = 8.8$ Å from the g_x-g_y plane to the center position of the C_{60} sphere.[34] From $\theta = 50°$, the center-to-center distance (r_{CC}) between the unpaired orbitals is found to be $r_{CC} = h/\cos\theta = 14$ Å. From the simple point-dipole approximation,[27] a distance of 16 Å gives the spin dipolar coupling of $D = -0.63$ mT, which is obtained by the SLE analysis. Considering the interchain delocalized hole distribution in Figure 5b to weaken the dipolar interaction, $r_{CC} = 14-15$ Å is a reasonable center separation to provide $D = -0.63$ mT[44] in Figure 3a.

For the CS state in Figure 5, $J = 6$ μT has been obtained by the SLE analysis of the TREPR spectra.[34,44] By using the configuration interaction mechanism[37−41] based on the Marcus ET theory, the $|V_{CR}| = 0.25$ cm^{-1} is characterized. This coupling is significantly smaller than the coupling ($V_{CT} \approx 100$ cm^{-1})[8] to induce the CT absorption and to cause the efficient electron injection from ^{1}P3HT* to $PC_{60}BM$ to generate the bound CT states. Such extremely small electronic interaction is consistent with the highly delocalized orbital distribution in the hole to suppress the orbital overlap between $P3AT^{+\bullet}$ and $PC_{60}BM^{-\bullet}$ in Figure 5b. Thus, it is concluded that the initial hole dissociation and delocalization after the photoinduced CT take place to produce the separated CS state with r_{CC} ranging from 15 to 24 Å at $T = 77$ K.

Supports of the Directional Charge Dissociations by Low-Temperature Transient Absorption Studies. The above low-temperature TREPR results tell us that the quick directional hole dissociations occur and that the holes are trapped at defined CS distances of ∼2 nm, undergoing the geminate CR deactivations at the defined and frozen orientations after the charge injections from ^{1}P3HT* to PCBM. One may be suspicious about the characterization of the defined conformations of the CS states in Figure 5 because of the anticipated heterogeneous molecular environment at the BHJ interfaces. Very recently, Hodgkiss et al.[49] have studied the transient absorption kinetics of photoinduced charges for the several blend materials at a wide range of temperatures. They characterized both the bound CT states and the separated CS states at cryogenic temperature. The bound CT states were assigned to be generated at more intimately mixed, disordered polymer/PCBM regions because this contribution was decreased by the thermal annealing procedures. These bound CT states deactivated within the 10 ns time regime at the cryogenic temperature, which is not detectable by the TREPR method because of the limited time resolution of ∼50 ns. Even if the intimately coupled photoinduced CT states are long-lived, such CT states should hold a pure singlet character due to the significantly large J by the orbital overlap and thus are not detectable by the EPR method because of lack of the $S-T_0$ interconversion in Figure 4. As for the separated CS states, the time traces of the transient absorption signals have been explained by the geminate CR process with the microsecond region for the frozen CS states distributed around $r_{CC} \approx 3$ nm. This is well compatible with the characterizations of the ∼2 nm separated electron−hole pairs, as shown in Figure 5b. Furthermore, Hodgkiss et al.[49] have also measured light-induced anisotropies in the transient absorption signals using the polarized pumps and probes and obtained the highly long-lived anisotropy for several microsecond regions on the separated CS states at the cryogenic temperature. This denotes that the initially separated electron−hole pairs have a memory of the direction of the transition dipole moment by the pump excitations, denoting that the initial carrier dissociations will take place in a defined direction and are frozen at the nanometer separations, as shown in Figure 5b.

From above arguments, it is indicated that, even if the $PC_{60}BM$ molecular conformations are heterogeneously distributed mainly by the free γ angles in Figure 5 at the polymer/$PC_{60}BM$ interfaces, the locally bound $\pi-\pi$ stacking structures by the polymer/$PC_{60}BM$ complexes are a clue to the efficient distant photocarrier generations at the domain interfaces.

Roles of the Frontier Orbitals on the Efficient Charge Dissociations. The quite small electronic interaction ($|V_{CR}| = 0.25$ cm^{-1}) in Figure 5b is in sharp contrast to the reported electronic couplings of $V_{CT} \approx 100$ cm^{-1} for the ultrafast charge injection dynamics from ^{1}P3HT* to $PC_{60}BM$.[8] Looking at the nanostructure of the P3HT/$PC_{60}BM$ complex in Figure 5, the difference in the $|V|$ is interpreted by the extreme decrease in the orbital overlap by the initial hole delocalization and dissociation in Figure 6. In the contact CT state, the larger orbital overlap is expected when the electron-accepting orbital of $PC_{60}BM$ employs the next upper level (b_{2u} orbital in the D_{2h} point group for $PC_{60}BM$)[8] to the LUMO (b_{1u}) in the ground state of $PC_{60}BM$ because the electron density in the b_{2u} orbital is highly distributed at the $PC_{60}BM$ bottom in the vicinity of the P3HT surface, as shown in Figure 6a.[58] Also, the initial orbital distribution of the hole should be localized near the $PC_{60}BM$ bottom in the contact CT to yield the large orbital overlap by the π-stacking structure.[8] This situation manifests the certain transition dipole moment[59,60] by the orbital overlap contributing to the optical CT band in Figure 5c.[12,57] Such a photoinduced CT state in Figure 6a will induce the large Coulomb attraction due to the *localized* positive and negative charge distributions at the surface of the P3AT aromatic plane. This is in line with a recent density functional theory calculation by Poluektov et al.;[3] when a negative point charge is placed on a thiophene oligomer surface, the spin density distribution of the polaron becomes significantly localized in the vicinity of the charge, which explains the experimental observations of the larger HF coupling of the positive polarons of P3HT in the presence of iodine counterions.

For the photocurrent generation, the hole in Figure 6a needs to escape from the strong CT binding whose energy is supposed

dx.doi.org/10.1021/jz5023202 | J. Phys. Chem. Lett. 2015, 6, 113−123

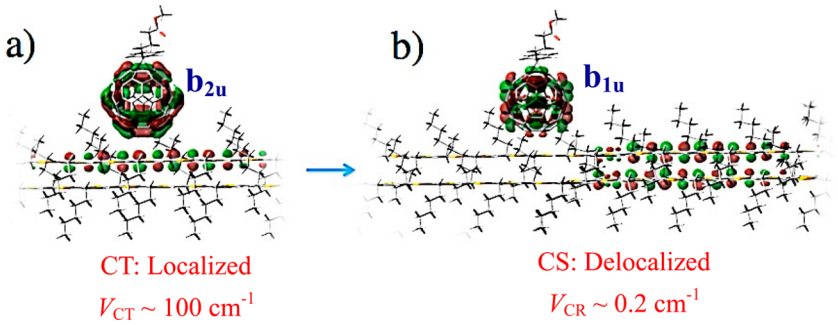

Figure 6. Schematic model[34] of the primary hole dissociation mechanism by the switches of the SOMOs from (a) the photoinduced contact CT state to (b) the delocalized CS state (Figure 5b) at the polymer crystalline/$PC_{60}BM$ interface at 77 K. At low temperature, the electron mobility of $PC_{60}BM^{-\bullet}$ is very small.[9] Thus, the position of the electron does not move, but the orbital is switched after the hole dissociation. In (a), LUMO+1 is represented as the dominant electron-accepting orbital (b_{2u} in the D_{2h} point group) in $PC_{60}BM$ to form the relaxed, photogenerated contact CT state with the large orbital overlap (V_{CT}) and with the large Coulomb stabilization by the localized interfacial charge distributions. The fast spin relaxations in (b) imply that the entropy is increased by the EP coupling after the hole dissociations. See the text for details.

to be 0.4 eV.[19] Thus, for the (a) → (b) process in Figure 6, the enthalpy change is described as $\Delta H_C \approx +0.4$ eV by the Coulomb attractions. The charge dissociation is however energetically feasible by switching the unpaired orbitals using (1) the delocalization[14] by the interchain hole distribution via the $\pi-\pi$ stacking in P3HT and (2) the internal conversion of the active singly occupied molecular orbital (SOMO) from the b_{2u} to the b_{1u} in the D_{2h} point group applied to $PC_{60}BM$.[58] In the former, the stabilization energy by creating the interchain polaron from the highest occupied molecular orbital (HOMO) of the single-chain P3HT is estimated to be ~0.3 eV by using the polaron absorption spectrum of the RR-P3HT film.[56] Due to the SOMO switching from the b_{2u} to the b_{1u} in $PC_{60}BM$, the orbital stabilization occurs by 0.05 eV.[8] Therefore, the enthalpy change is estimated to be $\Delta H_{orbit} \approx -0.4$ eV in total by the orbital switches evaluated *in the absence of the Coulomb attraction* between the charges.[34] The total enthalpy change is thus estimated to be $\Delta H_C + \Delta H_{orbit} \approx 0$ eV for the dissociation process.

The negative enthalpy changes by the orbital switches are used to overcome the destabilization by the weakened Coulomb attraction for the electron–hole dissociations.

The negative enthalpy changes by the orbital switches are used to overcome the destabilization by the weakened Coulomb attraction for the electron–hole dissociations.

It is also emphasized in Figure 6b that the significantly decreased electronic interaction of $V_{CR} \approx 0.2$ cm^{-1} with respect to the V_{CT} is coincident with the b_{1u} character in the $PC_{60}BM$; because the electron density of the b_{1u} orbital is distributed along the equatorial $X-Y$ position bisecting the C_{60} sphere, the overlap between the unpaired orbitals is highly inhibited, as shown in Figure 5a and b. It is concluded that not only the productions of the separated electron–hole pair but also the orbital configuration changes are key to the prevention of the energy-wasting CR after the interfacial CT reaction.

Connection between the Molecular Motion and the Geometry of the Distant CS State. The representative geometry of the electron–hole pairs is obtained by the SLE analysis of the TREPR spectra, as shown in Figure 5. From the recent transient absorption measurements,[49] it has also been revealed that such CS states are geometrically frozen for more than microseconds at the cryogenic temperature. It should however be noted that the fast spin relaxations ($T_1 \approx 0.5$ μs as the spin–lattice relaxation time and T_2 of 10–50 ns as the transverse relaxation time) are required to fully reproduce time developments of the EPR spectra even at $T = 77$ K.[34,44] This denotes that the positions and orientations of the unpaired spins are fluctuated[45] around the structure in Figure 5b. For the as-spun RR-P3HT/$PC_{60}BM$, a fast $S-T_0$ dephasing time ($T_{23} = 1.2$ μs)[44] is required in Figure 4 to completely reproduce the delay time dependence of the TREPR spectra. Because the $S-T_0$ dephasing is induced by the fluctuations of the exchange and the dipolar couplings,[51] the libration motions or the spatial distribution in the unpaired spins are conclusive. This is also consistent with the recent low-temperature transient absorption measurements by which the distance distributions in the separated electron–hole pairs were concluded.[49] As for the spin–lattice relaxation, $T_1 \approx 0.5$ μs (as characterized by the decays of the initial emissive $T_0 \rightarrow T_-$ transitions to the absorptive thermal equilibrium transitions in Figure 3j) at 77 K for the blend films is 10 times smaller than $T_1 = 5$ μs reported for a distant CS state of a zinc porphyrin–fullerene-linked dyad molecule in a frozen solution (91 K).[42] Also, the T_1 of 0.5 μs is smaller than $T_1 = 1$ μs obtained for a distant CS state ($ZnP^{+\bullet}-H_2P-C_{60}^{-\bullet}$) of a zinc porphyrin-free base porphyrin–fullerene triad in benzonitrile at room temperature.[43] Thus, the fast spin relaxations in the present systems are explained by the effective lattice librations by the electron–phonon (EP) coupling in the organic semiconductors.[61] The pseudorotational mobility between the b_{1u} and the b_{2u} in $PC_{60}BM^{-\bullet}$ has also been explained by the phonon-assisted hopping and may play a role in the fast spin relaxations.[34,61]

After the treatment of the thermal annealing of the blend film, the dipolar coupling became weaker from −0.63 to −0.46 mT,[44] indicating that the hole is more separated at the domain interface. The angle of θ has been decreased from 50 to 44° by the annealing, denoting that $P3HT^{+\bullet}$ has been separated not to the intrachain direction in the conjugated polymer but to the interchain direction by the π-stackings, as shown in Figure 7.[44] In the RR-P3DDT/$PC_{60}BM$ system, the dipolar coupling became much weaker (−0.20 mT), while θ was decreased from 50 to 45° on the as-spun films.[44] These results also denote that the interchain hole dissociation is taking place toward the π-stacking direction at the RR-P3DDT/$PC_{60}BM$ interface. The hole

dx.doi.org/10.1021/jz5023202 | J. Phys. Chem. Lett. 2015, 6, 113–123

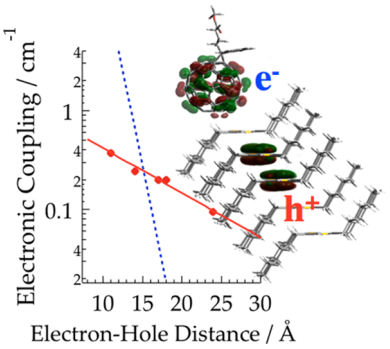

Figure 7. Semilog plot (red) of $|V_{CR}|$ versus r_{CC} of the electron−hole pairs in the several P3AT/$PC_{60}BM$ (1:1) blend materials prepared from the 1,2-dichlorobenzene solutions. β_e = 0.2 $Å^{-1}$ is obtained[44] as the attenuation factor in the exponential decay of the electronic coupling, as shown by the red line. The blue dotted line is obtained for the reported CS states of the DNA hairpin systems of $G^{+\bullet}$-$(T)_m$-$S^{-\bullet}$ by using β_e = 0.9 $Å^{-1}$ and $|V_{CR}| \approx 20$ cm^{-1} at r_{CC} = 10 Å.[67,68]

dissociations induced by the increased alkyl side chains in P3AT strongly indicate a coupling of the hole to the librations (phonon)[61,62] of the P3AT crystalline domains; the increase in the side chain's number promotes the motions of the alkyl side chains due to the significant increase in the vibrational modes that couple to the unpaired orbital. Such EP coupling contributes to the instantaneous interchain mobility for the hole dissociations.[62] The thermal annealing effect on the hole dissociation is similarly explained by the side chain motions in P3AT, as follows. Recent X-ray diffraction analyses of the RR-P3HT/$PC_{60}BM$ blend films reported that the P3HT domain size is increased by the thermal annealing due to a permanent lamellar stretching just along the alkyl-stacking direction.[54] This lamellar stretching can induce the disordered conformations of the end group ($-CH_3$) in the hexyl chain because of the lack of rotational restrictions in $-CH_3$ by the alkyl-stacking interactions.[63] Such disordered motions by the side chains can enhance both the EP coupling and the entropy for the hole dissociations to stabilize the more separated electron−hole pairs than in the RR-P3HT/$PC_{60}BM$ blend.[44]

Contrary to the separated CS states (Figure 6b) in which the distributions are created in the conformations and in the distances by the EP couplings, the contact CT states (Figure 6a) will not have such spatial distributions; the strong Coulomb binding will freeze both the interchain disordered motions and the b_{2u} orbital character in $PC_{60}BM^{-\bullet}$.[34] Thus, the entropy enhancement ($\Delta S > 0$) is conclusive in Figure 6, contributing to the exothermic electron−hole dissociation by the negative free-energy change as determined by $\Delta G_{CS} = \Delta H_C + \Delta H_{orbit} - T\Delta S$.

The enhanced disorder orbital motions after the charge dissociation will contribute to the increase in the entropy, promoting the initial dissociation as the exothermic process via the contact CT state.

The enhanced disorder orbital motions after the charge dissociation will contribute to the increase in the entropy, promoting the initial dissociation as the exothermic process via the contact CT state.

Energetic Pathway of Photoinduced Charge Dissociation via CT. Instead of the above dissociation scheme in Figure 6, one might expect that one-step distant ET from the delocalized excition in the polymer crystalline region to PCBM may result in the highly separated electron−hole pair in Figure 5 without going through the CT state. When this scenario is adopted, the electronic coupling of V_{CR} = 0.2 cm^{-1} obtained here on the CS state is roughly applied also for the forward ET process. This coupling magnitude is too small to explain the highly quick CS state generation at the ultrafast time scales[18] even if the ET is highly exothermic. It is thus concluded from the CS geometry and from the electronic coupling that the photoinduced charge dissociation takes place accompanying the quick delocalization via the contact CT state at the polymer crystalline/PCBM interface. It is however not clear from the present experiments whether the dissociation proceeds via the energetically higher CT[18] or via the relaxed CT.[15] Nevertheless, in the P3HT/PCBM system, the IQE (~80%) is reported to be essentially independent of the excitation energy.[12] Also, the dissociation via the stabilized contact CT is now revealed to be exothermic. As a consequence, it is reasonably implicated that the relaxed CT pathway as shown in Figure 6 dominates the carrier dissociation.

It is thus concluded from the CS geometry and from the electronic coupling that the photoinduced charge dissociation takes place accompanying the quick delocalization via the contact CT state at the polymer crystalline/PCBM interface.

Nature of the Electronic Conduction on the Interfacial Electron−Hole Pairs. Because the OPV cells function at room temperature, one may consider that the present low-temperature characterizations of the geometry, the motion, and the electronic couplings cannot be applied to understand the molecular mechanism of the initial photocurrent generations. Also, the standard EPR measurements using the phase-sensitive detection have been utilized to monitor the carrier defects and traps that disrupt the photocurrent rather than to elucidate the mechanism of the initial photocurrent, as reported by Marumoto et al.[64] It is highly required to evaluate the trap depth of the interfacial transient CS state for the identification of the electronic conduction characters influenced by the environment of the organic semiconductors at the D/A domain interfaces.

From the 2J parameters, one can estimate the $|V_{CR}|$ values using the configuration interaction model as described above. The $|V_{CR}|$ values have been plotted with respect to the r_{CC} values in Figure 7, together with the $|V_{CR}|$ reported for the cast films of the regiorandom-P3HT/$PC_{60}BM$ and of the RR-P3HT/$PC_{60}BM$ blend.[34] From the semilog plot in Figure 7, it is evident that the electronic coupling decays by the single-exponential function as r_{CC} is increased. Such decays have been characterized by the attenuation factor of β_e in $|V_{CR}| = V_0 \exp\{-\beta_e (r_{CC} - r_0)/2\}$, as shown by the red line in Figure 7.[65,66] The least-squares fitting (the red line) of the plots yields β_e = 0.2 $Å^{-1}$. In DNA hairpin systems that generate the photoinduced CS states of $G^{+\bullet}$-$(T)_m$-$S^{-\bullet}$ in which S, T and G represent stacking stillbene, thymine, and guanine bases, respectively, Lewis et al.[67] have

dx.doi.org/10.1021/jz5023202 | J. Phys. Chem. Lett. 2015, 6, 113−123

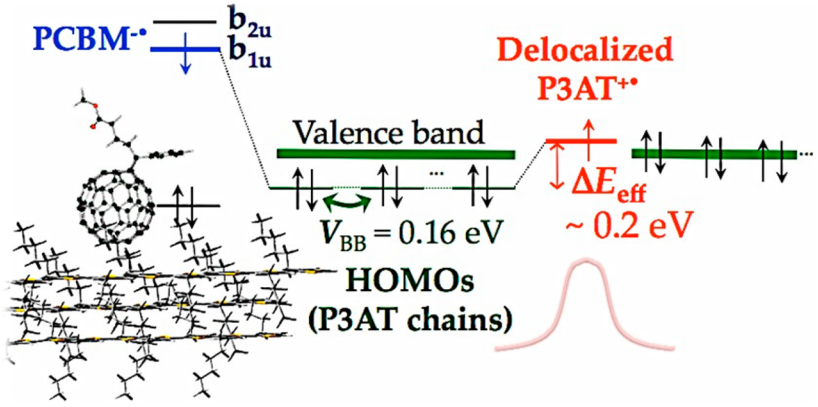

Figure 8. Diagram of the orbital levels of the interfacial CS states distributed at $r_{CC} \approx 2$ nm at $T = 77$ K. Using the superexchange model, the tunneling barrier ($\Delta E_{eff} \approx 0.2$ eV) has been estimated from $\beta_e = 0.2$ Å^{-1} in Figure 7 with respect to the HOMO levels of the bridging single polymer units. This indicates that the interchain delocalized hole in Figure 7 is located close to the level of the top of the valence band generated by the V_{BB} interactions in the P3AT crystalline domains. At elevated temperature, this delocalized transient hole will be detrapped and escape from the weak Coulomb attraction by the separated $PC_{60}BM^{-\bullet}$ efficiency, generating the photocurrent in the OPV cell.

obtained $\beta_e = 0.9$ Å^{-1} for the CR processes. By using $|V_{CR}| \approx 20$ cm^{-1} reported for $G^{+\bullet}$-$(T)_2$-$S^{-\bullet}$, where the interspin distance is $r_{CC} = 10$ Å separated by the two π-stacking thymines,[68] the dotted blue line is drawn as in Figure 7. At closer distances ($r_{CC} <$ 15 Å), the magnitudes of the electronic coupling are larger in the DNA hairpin systems than those in the present interfacial CS systems. This is reasonably explained by the significant difference in the delocalization sizes of the unpaired orbitals. Because the unpaired orbitals are extensively distributed in the buckyballs and in the organic conjugated polymers[3] in the spaces of ~nm^3, as shown in Figure 5, the orbital overlap will be significantly weak in these CS systems, as explained above. On the other hand, because the molecular sizes of stillbene and guanine are much smaller, the localized orbital distributions will generate the extremely larger overlap when the interspin separation is small. This strongly supports the validities of the absolute values of $|V_{CR}|$ in Figure 7 obtained by the TREPR analyses.[34]

For $r_{CC} > 15$ Å, the electronic coupling is significantly larger in the interfacial CS states of the OPV blend films, representing the superior electronic conduction properties by the organic semiconductors due to the small attenuation factor of $\beta_e = 0.2$ Å^{-1}. Using the McConnell's electron-tunneling model, β_e is approximated as follows[66,69]

$$\beta_e = \frac{2}{d_{BB}} \ln\left(\frac{\Delta E_{eff}}{V_{BB}}\right) \quad (1)$$

where d_{BB} and V_{BB} are the bridge-to-bridge stacking distance and the transfer integral between the bridging chromophores, respectively. ΔE_{eff} is the tunneling energy gap for the holes to oxidize the bridge units. $d_{BB} = 3.4$ Å and $V_{BB} = 0.16$ eV are estimated for the π-stacking distances and for the π-stacking interactions between the bridge molecules, respectively, both in the DNAs[70] and in the crystalline domains of P3AT.[71] From eq 1, $\Delta E_{eff} = 0.7$ eV is evaluated in the DNA hairpins. This is consistent with the oxidation potential difference between T and G, indicating that the $G^{+\bullet}$ is the deep trap site with respect to the bridge unit of T_m. In the interfacial CS system in the blend film, $\Delta E_{eff} = 0.2$ eV is evaluated as the tunneling barrier from the delocalized holes in the P3AT region to the HOMOs of the single P3AT chains by using $\beta_e = 0.2$ Å^{-1}, as shown in Figure 8. This tunneling energy gap is comparable to V_{BB} and is consistent with the dimer polaron model[56] that explains the shift of the optical absorption band of the delocalized polarons by the π-stackings in the P3HT region. The above small tunneling barrier with $\Delta E_{eff} \approx V_{BB}$ implies that the transient holes in Figure 7 are energetically located at the level close to the top of the valence band in the P3AT crystalline domain, as shown in Figure 8, because the higher level of the valence band can be generated also by the V_{BB} interactions between the single HOMOs in the crystalline region, as shown in Figure 8. Such a quite small energy difference between the delocalized unpaired orbital and the top of the valence band strongly implies that the transient CS states are in the shallow traps for the unpaired orbitals in the P3AT domains at $T = 77$ K. This indicates that the transient hole spatially distributed as in Figure 8 will become a photocarrier contributing to the predominant photocurrent at room temperature because the trapped hole can be detrapped at higher temperature.[72] The above argument is very consistent with the recent temperature dependence of the transient absorption kinetics as studied by Hodgkiss et al.;[49] the highly long-lived transient absorption anisotropy on the separated CS states at low temperature quickly disappears when the temperature is elevated to room temperature, denoting that the weakly bound carriers are detrapped and diffuse in the photoactive layer. This is also in line with the report that the photocurrent density is dramatically increased by more than an order of magnitude when the temperature is increased from ~100 to 300 K in the solar cell employing the RR-P3HT/$PC_{60}BM$ film.[12]

The highly long-range tunneling character originating from the shallow trap depth with respect to the valence band will be a key to the efficient photocarrier conduction in the OPV cells.

The highly long-range tunneling character originating from the shallow trap depth with respect to the valence band will be a key to the efficient photocarrier conduction in the OPV cells.

Perspective. For deeper understandings of the directions and of the trap depths for efficient interfacial carrier conductions, it is important to investigate temperature and morphology effects on the CS geometry and the electronic coupling. Also, it is highly

dx.doi.org/10.1021/jz5023202 | J. Phys. Chem. Lett. 2015, 6, 113−123

required to explore in details the geometries and the β_e values of the separated electron−hole pairs for the low-band-gap polymer systems[3,4] to elucidate the mechanism of the recent developments of the higher incident photon to current efficiency (IPCE). Because the transient absorption anisotropies have been reported by using the polarized pumps and probes on the several separated carriers,[49] the magnetophotoselection measurements[73] of the distant CS state systems will also be very powerful to characterize more details of the geometries and the electronic couplings in the photoactive layers.

In conclusion, we have shown that the low-temperature TREPR measurements are powerful to characterize the geometry, the motions, and the electronic conduction properties of the interfacial transient electron−hole pairs in the OVP materials to unveil the underlying mechanism of the efficient photocurrent generations. These structural and electronic characteristics are essential keys to the evaluations, the designs, and the developments of the highly efficient artificial solar energy conversion systems employing the organic molecules.

AUTHOR INFORMATION

Corresponding Author

*E-mail: ykobori@kitty.kobe-u.ac.jp.

Notes

The authors declare no competing financial interest.

Biographies

Yasuhiro Kobori is a Professor of Chemistry at Kobe University. He received his Ph.D. in Chemistry in 1998 under the supervision of Kinichi Obi from Tokyo Institute of Technology. Before joining Kobe University in 2013, he was employed at Tohoku University from 1996 to 2002, at The University of Chicago from 2002 to 2006, and at Shizuoka University from 2006 to 2013. His research interest includes mechanisms of charge generations in photosynthetic proteins, organic photovoltaic systems, and molecular wires for development of the efficient light−energy conversion systems. Website: http://www.chem.sci.kobe-u.ac.jp/en/staffE/KoboriE/

Taku Miura is a graduate student in the Kobori group in the Department of Chemistry, Graduate School Science at Kobe University. His research interest includes EPR investigation of the geometries of the photoinduced carriers in the OPV materials.

ACKNOWLEDGMENTS

The authors thank Prof. Hisao Murai (Shizuoka University), Prof. Hideo Ohkita (Kyoto University), Prof. Kazuhiro Marumoto (Tsukuba University), and Prof. Kiminior Maeda (Saitama University) for their useful support and discussions. This work was supported in part by a Grant-in-Aid for Scientific Research (No. 25288004 and 26620065) from the Ministry of Education, Culture, Sports, Science and Technology, Japan.

ABBREVIATIONS

OPV, organic photovoltaic; BHJ, bulk heterojunction; P3AT, poly(3-alkylthiophene); $PC_{60}BM$, [6,6]-C_{61}-butyric acid methyl ester; PCE, power conversion efficiency; IQE, internal quantum efficiency; CR, charge recombination; V_{CR}, electronic coupling matrix element for charge recombination; TREPR, time-resolved electron paramagnetic resonance; HFI, hyperfine interaction; r_{CC}, center-to-center separation between electron spins; $2J$, spin−spin exchange coupling; D, electron spin−spin dipolar interaction; $\boldsymbol{d}$, interspin vector; SCRP, spin-correlated radical pair; RR-P3DDT, regioregular poly(3-dodecylthiophene-2,5-diyl); SLE, stochastic-Liouville equation; EP, electron−phonon; β_e, attenuation factor in distance dependence of V_{CR}; V_{BB}, transfer integral between bridging chromophores; ΔE_{eff}, tunneling energy gap for a hole to oxidize a bridge unit; IPCE, incident photon to current efficiency

REFERENCES

(1) Yu, G.; Gao, J.; Hummelen, J. C.; Wudl, F.; Heeger, A. J. Polymer photovoltaic cells — Enhanced efficiencies via a network of internal donor−acceptor heterojunctions. *Science* **1995**, *270*, 1789−1791.

(2) Kim, Y.; Cook, S.; Tuladhar, S. M.; Choulis, S. A.; Nelson, J.; Durrant, J. R.; Bradley, D. D. C.; Giles, M.; Mcculloch, I.; Ha, C. S.; Ree, M. A strong regioregularity effect in self-organizing conjugated polymer films and high-efficiency polythiophene:fullerene solar cells. *Nat. Mater.* **2006**, *5*, 197−203.

(3) Niklas, J.; Mardis, K. L.; Banks, B. P.; Grooms, G. M.; Sperlich, A.; Dyakonov, V.; Beaupre, S.; Leclerc, M.; Xu, T.; Yu, L. P.; Poluektov, O. G. Highly-efficient charge separation and polaron delocalization in polymer−fullerene bulk-heterojunctions: A comparative multi-frequency EPR and DFT study. *Phys. Chem. Chem. Phys.* **2013**, *15*, 9562−9574.

(4) Osaka, I.; Saito, M.; Koganezawa, T.; Takimiya, K. Thiophene−thiazolothiazole copolymers: Significant impact of side chain composition on backbone orientation and solar cell performances. *Adv. Mater.* **2014**, *26*, 331−338.

(5) Schumann, S.; Da Campo, R.; Illy, B.; Cruickshank, A. C.; McLachlan, M. A.; Ryan, M. P.; Riley, D. J.; McComb, D. W.; Jones, T. S. Inverted organic photovoltaic devices with high efficiency and stability based on metal oxide charge extraction layers. *J. Mater. Chem.* **2011**, *21*, 2381−2386.

(6) Guo, J. M.; Ohkita, H.; Benten, H.; Ito, S. Charge generation and recombination dynamics in poly(3-hexylthiophene)/fullerene blend films with different regioregularities and morphologies. *J. Am. Chem. Soc.* **2010**, *132*, 6154−6164.

(7) Saeki, A.; Yoshikawa, S.; Tsuji, M.; Koizumi, Y.; Ide, M.; Vijayakumar, C.; Seki, S. A versatile approach to organic photovoltaics evaluation using white light pulse and microwave conductivity. *J. Am. Chem. Soc.* **2012**, *134*, 19035−19042.

(8) Liu, T.; Troisi, A. Absolute rate of charge separation and recombination in a molecular model of the P3HT/PCBM interface. *J. Phys. Chem. C* **2011**, *115*, 2406−2415.

(9) Grzegorczyk, W. J.; Savenije, T. J.; Dykstra, T. E.; Piris, J.; Schins, J. M.; Siebbeles, L. D. A. Temperature-independent charge carrier photogeneration in P3HT−PCBM blends with different morphology. *J. Phys. Chem. C* **2010**, *114*, 5182−5186.

(10) Bakulin, A. A.; Rao, A.; Pavelyev, V. G.; van Loosdrecht, P. H. M.; Pshenichnikov, M. S.; Niedzialek, D.; Cornil, J.; Beljonne, D.; Friend, R. H. The role of driving energy and delocalized states for charge separation in organic semiconductors. *Science* **2012**, *335*, 1340−1344.

(11) Choi, J. H.; Son, K. I.; Kim, T.; Kim, K.; Ohkubo, K.; Fukuzumi, S. Thienyl-substituted methanofullerene derivatives for organic photovoltaic cells. *J. Mater. Chem.* **2010**, *20*, 475−482.

(12) Lee, J.; Vandewal, K.; Yost, S. R.; Bahlke, M. E.; Goris, L.; Baldo, M. A.; Manca, J. V.; Van Voorhis, T. Charge transfer state versus hot exciton dissociation in polymer−fullerene blended solar cells. *J. Am. Chem. Soc.* **2010**, *132*, 11878−11880.

(13) Ko, S. W.; Hoke, E. T.; Pandey, L.; Hong, S. H.; Mondal, R.; Risko, C.; Yi, Y. P.; Noriega, R.; McGehee, M. D.; Bredas, J. L.; Salleo, A.; Bao, Z. A. Controlled conjugated backbone twisting for an increased open-circuit voltage while having a high short-circuit current in poly(hexylthiophene) derivatives. *J. Am. Chem. Soc.* **2012**, *134*, 5222−5232.

(14) Murthy, D. H. K.; Gao, M.; Vermeulen, M. J. W.; Siebbeles, L. D. A.; Savenije, T. J. Mechanism of mobile charge carrier generation in blends of conjugated polymers and fullerenes: significance of charge delocalization and excess free energy. *J. Phys. Chem. C* **2012**, *116*, 9214−9220.

(15) Vandewal, K.; Albrecht, S.; Hoke, E. T.; Graham, K. R.; Widmer, J.; Douglas, J. D.; Schubert, M.; Mateker, W. R.; Bloking, J. T.; Burkhard, G. F.; Sellinger, A.; Frechet, J. M. J.; Amassian, A.; Riede, M. K.; McGehee, M. D.; Neher, D.; Salleo, A. Efficient charge generation by relaxed charge-transfer states at organic interfaces. *Nat. Mater.* **2014**, *13*, 63−68.
(16) Grancini, G.; Polli, D.; Fazzi, D.; Cabanillas-Gonzalez, J.; Cerullo, G.; Lanzani, G. Transient absorption imaging of P3HT:PCBM photovoltaic blend: Evidence for interfacial charge transfer state. *J. Phys. Chem. Lett.* **2011**, *2*, 1099−1105.
(17) Deibel, C.; Strobel, T.; Dyakonov, V. Role of the charge transfer state in organic donor−acceptor solar cells. *Adv. Mater.* **2010**, *22*, 4097−4111.
(18) Grancini, G.; Maiuri, M.; Fazzi, D.; Petrozza, A.; Egelhaaf, H. J.; Brida, D.; Cerullo, G.; Lanzani, G. Hot exciton dissociation in polymer solar cells. *Nat. Mater.* **2013**, *12*, 29−33.
(19) Clarke, T. M.; Durrant, J. R. Charge photogeneration in organic solar cells. *Chem. Rev.* **2010**, *110*, 6736−6767.
(20) Murai, H.; Imamura, T.; Obi, K. Time-resolved electron-spin-resonance detection of benzophenone nπ^* triplet-state in glassy matrices at 77 K. *Chem. Phys. Lett.* **1982**, *87*, 295−298.
(21) Closs, G. L.; Forbes, M. D. E.; Norris, J. R. Spin-polarized electron-paramagnetic resonance-spectra of radical pairs in micelles: Observation of electron spin−spin interactions. *J. Phys. Chem.* **1987**, *91*, 3592−3599.
(22) Franco, L.; Ruzzi, M.; Corvaja, C. Time-resolved electron paramagnetic resonance of photoinduced ion pairs in blends of polythiophene and fullerene derivatives. *J. Phys. Chem. B* **2005**, *109*, 13431−13435.
(23) Hore, P. J.; Hunter, D. A.; McKie, C. D.; Hoff, A. J. Electron paramagnetic resonance of spin-correlated radical pairs in photosynthetic reactions. *Chem. Phys. Lett.* **1987**, *137*, 495−500.
(24) Norris, J. R.; Morris, A. L.; Thurnauer, M. C.; Tang, J. A general-model of electron-spin polarization arizing from the interactions within radical pairs. *J. Chem. Phys.* **1990**, *92*, 4239−4249.
(25) Kothe, G.; Weber, S.; Bittl, R.; Ohmes, E.; Thurnauer, M. C.; Norris, J. R. Trasien EPR of light-induced radical pairs in plant photosystem-I — Observation of quantum beats. *Chem. Phys. Lett.* **1991**, *186*, 474−480.
(26) Prisner, T. F.; Vanderest, A.; Bittl, R.; Lubitz, W.; Stehlik, D.; Mobius, K. Time-resolved W-band (95 GHZ) EPR spectroscopy of Zn-substituted reaction centers of *Rhodobacter sphaeroides* R-26. *Chem. Phys.* **1995**, *194*, 361−370.
(27) Till, U.; Klenina, I. B.; Proskuryakov, I. I.; Hoff, A. J.; Hore, P. J. Recombination Dynamics and EPR Spectra of the Primary Radical Pair in Bacterila Photosynthetic Reaction Centers with Blocked Electron Transfer to the Primary Acceptor. *J. Phys. Chem. B* **1997**, *101*, 10939−10948.
(28) vanderEst, A.; Prisner, T.; Bittl, R.; Fromme, P.; Lubitz, W.; Mobius, K.; Stehlik, D. Time-resolved X-, K-, and W-band EPR of the radical pair state $P_{700}^{\bullet+}A_1^{\bullet}$ of photosystem I in comparison with $P_{865}^{\bullet+}Q_A^{\bullet-}$ in bacterial reaction centers. *J. Phys. Chem. B* **1997**, *101*, 1437−1443.
(29) Carbonera, D.; Di Valentin, M.; Corvaja, C.; Agostini, G.; Giacometti, G.; Liddell, P. A.; Kuciauskas, D.; Moore, A. L.; Moore, T. A.; Gust, D. EPR investigation of photoinduced radical pair formation and decay to a triplet state in a carotene−porphyrin−fullerene triad. *J. Am. Chem. Soc.* **1998**, *120*, 4398−4405.
(30) Carrington, A.; McLachlan, A. D. *Introduction to Magnetic Resonance*; Harper & Row: New York, 1967.
(31) Poluektov, O. G.; Filippone, S.; Martin, N.; Sperlich, A.; Deibel, C.; Dyakonov, V. Spin signatures of photogenerated radical anions in polymer−[70]fullerene bulk heterojunctions: high frequency pulsed EPR spectroscopy. *J. Phys. Chem. B* **2010**, *114*, 14426−14429.
(32) Krinichnyi, V. I.; Yudanova, E. I.; Spitsina, N. G. Light-induced electron paramagnetic resonance study of poly(3-alkylthiophene)/fullerene composites. *J. Phys. Chem. C* **2010**, *114*, 16756−16766.
(33) Behrends, J.; Sperlich, A.; Schnegg, A.; Biskup, T.; Teutloff, C.; Lips, K.; Dyakonov, V.; Bittl, R. Direct detection of photoinduced charge transfer complexes in polymer fullerene blends. *Phys. Rev. B* **2012**, *85*, 125206.
(34) Kobori, Y.; Noji, R.; Tsuganezawa, S. Initial molecular photocurrent: Nanostructure and motion of weakly bound charge-separated state in organic photovoltaic interface. *J. Phys. Chem. C* **2013**, *117*, 1589−1599.
(35) Kandrashkin, Y. E.; Salikhov, K. M.; van der Est, A.; Stehlik, D. Electron spin polarization in consecutive spin-correlated radical pairs: Application to short-lived and long-lived precursors in type 1 photosynthetic reaction centres. *Appl. Magn. Reson.* **1998**, *15*, 417−447.
(36) Calvo, R.; Abresch, E. C.; Bittl, R.; Feher, G.; Hofbauer, W.; Isaacson, R. A.; Lubitz, W.; Okamura, M. Y.; Paddock, M. L. EPR study of the molecular and electronic structure of the semiquinone biradical $Q_A^{-\bullet}Q_B^{-\bullet}$ in photosynthetic reaction centers from *Rhodobacter sphaeroides*. *J. Am. Chem. Soc.* **2000**, *122*, 7327−7341.
(37) Anderson, P. W. New approach to the theory of superexchange interactions. *Phys. Rev.* **1959**, *115*, 2−13.
(38) Michelbeyerle, M. E.; Bixon, M.; Jortner, J. Interrelationship between primary electron-transfer dynamics and magnetic-interactions in photosynthetic reaction centers. *Chem. Phys. Lett.* **1988**, *151*, 188−194.
(39) Bixon, M.; Jortner, J.; Michelbeyerle, M. E.; Ogrodnik, A. A superexchange mechanism for the primary charge separation in photosynthetic reaction centers. *Biochim. Biophys. Acta* **1989**, *977*, 273−286.
(40) Kobori, Y.; Sekiguchi, S.; Akiyama, K.; Tero-Kubota, S. Chemically induced dynamic electron polarization study on the mechanism of exchange interaction in radical ion pairs generated by photoinduced electron transfer reactions. *J. Phys. Chem. A* **1999**, *103*, 5416−5424.
(41) Goldsmith, R. H.; Sinks, L. E.; Kelley, R. F.; Betzen, L. J.; Liu, W. H.; Weiss, E. A.; Ratner, M. A.; Wasielewski, M. R. Wire-like charge transport at near constant bridge energy through fluorene oligomers. *Proc. Natl. Acad. Sci. U.S.A.* **2005**, *102*, 3540−3545.
(42) Kobori, Y.; Fuki, M.; Murai, H. Electron spin polarization transfer to the charge-separated state from locally excited triplet configuration: Theory and its application to characterization of geometry and electronic coupling in the electron donor−acceptor system. *J. Phys. Chem. B* **2010**, *114*, 14621−14630.
(43) Kobori, Y.; Yamauchi, S.; Akiyama, K.; Tero-Kubota, S.; Imahori, H.; Fukuzumi, S.; Norris, J. R. Primary charge-recombination in an artificial photosynthetic reaction center. *Proc. Natl. Acad. Sci. U.S.A.* **2005**, *102*, 10017−10022.
(44) Miura, T.; Aikawa, M.; Kobori, Y. Time-resolved EPR study of electron−hole dissociations influenced by alkyl side chains at the photovoltaic polyalkylthiophene:PCBM interface. *J. Phys. Chem. Lett.* **2014**, *5*, 30−35.
(45) D'avino, G.; Mothy, S.; Muccioli, L.; Zannoni, C.; Wang, L. J.; Cornil, J.; Beljonne, D.; Castet, F. Energetics of electron−hole separation at P3HT/PCBM heterojunctions. *J. Phys. Chem. C* **2013**, *117*, 12981−12990.
(46) Pensack, R. D.; Guo, C.; Vakhshouri, K.; Gomez, E. D.; Asbury, J. B. Influence of acceptor structure on barriers to charge separation in organic photovoltaic materials. *J. Phys. Chem. C* **2012**, *116*, 4824−4831.
(47) Baranovskii, S. D.; Wiemer, M.; Nenashev, A. V.; Jansson, F.; Gebhardt, F. Calculating the efficiency of exciton dissociation at the interface between a conjugated polymer and an electron acceptor. *J. Phys. Chem. Lett.* **2012**, *3*, 1214−1221.
(48) Tada, A.; Geng, Y. F.; Wei, Q. S.; Hashimoto, K.; Tajima, K. Tailoring organic heterojunction interfaces in bilayer polymer photovoltaic devices. *Nat. Mater.* **2011**, *10*, 450−455.
(49) Barker, A. J.; Chen, K.; Hodgkiss, J. M. Distance distributions of photogenerated charge pairs in organic photovoltaic cells. *J. Am. Chem. Soc.* **2014**, *136*, 12018−12026.
(50) Kothe, G.; Weber, S.; Ohmes, E.; Thurnauer, M. C.; Norris, J. R. Transient EPR of light-induced spin-correlated radical pairs — Manifestiation of zero-quantum coherence. *J. Phys. Chem.* **1994**, *98*, 2706−2712.

(51) Fukuju, T.; Yashiro, H.; Maeda, K.; Murai, H.; Azumi, T. Singlet-born SCRP observed in the photolysis of tetraphenylhydrazine in an SDS micelle: Time dependence of the population of the spin states. *J. Phys. Chem. A* **1997**, *101*, 7783−7786.
(52) Watanabe, S.-i.; Tanaka, H.; Kuroda, S.-i.; Toda, A.; Nagano, S.; Seki, T.; Kimoto, A.; Abe, J. Electron spin resonance observation of field-induced charge carriers in ultrathin-film transistors of regioregular poly(3-hexylthiophene) with controlled in-plane chain orientation. *Appl. Phys. Lett.* **2010**, *96*, 173302.
(53) Kayunkid, N.; Uttiya, S.; Brinkmann, M. Structural model of regioregular poly(3-hexylthiophene) obtained by electron diffraction analysis. *Macromolecules* **2010**, *43*, 4961−4967.
(54) Lilliu, S.; Agostinelli, T.; Pires, E.; Hampton, M.; Nelson, J.; Macdonald, J. E. Dynamics of crystallization and disorder during annealing of P3HT/PCBM bulk heterojunctions. *Macromolecules* **2011**, *44*, 2725−2734.
(55) Li, G.; Shrotriya, V.; Huang, J. S.; Yao, Y.; Moriarty, T.; Emery, K.; Yang, Y. High-efficiency solution processable polymer photovoltaic cells by self-organization of polymer blends. *Nat. Mater.* **2005**, *4*, 864−868.
(56) Jiang, X. M.; Österbacka, R.; Korovyanko, O.; An, C. P.; Horovitz, B.; Janssen, R. A. J.; Vardeny, Z. V. Spectroscopic studies of photoexcitations in regioregular and regiorandom polythiophene films. *Adv. Funct. Mater.* **2002**, *12*, 587−597.
(57) Tvingstedt, K.; Vandewal, K.; Gadisa, A.; Zhang, F. L.; Manca, J.; Inganas, O. Electroluminescence from charge transfer states in polymer solar cells. *J. Am. Chem. Soc.* **2009**, *131*, 11819−11824.
(58) Kanai, Y.; Grossman, J. C. Insights on interfacial charge transfer across P3HT/fullerene photovoltaic heterojunction from ab initio calculations. *Nano Lett.* **2007**, *7*, 1967−1972.
(59) Imahori, H.; Tkachenko, N. V.; Vehmanen, V.; Tamaki, K.; Lemmetyinen, H.; Sakata, Y.; Fukuzumi, S. An extremely small reorganization energy of electron transfer in porphyrin−fullerene dyad. *J. Phys. Chem. A* **2001**, *105*, 1750−1756.
(60) Gould, I. R.; Young, R. H.; Mueller, L. J.; Albrecht, A. C.; Farid, S. Electronic structures of exciplexes and excited charge-transfer complexes. *J. Am. Chem. Soc.* **1994**, *116*, 8188−8199.
(61) Krinichnyi, V. I.; Yudanova, E. I. Structural effect of electron acceptor on charge transfer in poly(3-hexylthiophene)/methanofullerene bulk heterojunctions. *Sol. Energy Mater. Sol. Cells* **2011**, *95*, 2302−2313.
(62) Vukmirović, N.; Wang, L. W. Carrier hopping in disordered semiconducting polymers: How accurate is the Miller−Abrahams model? *Appl. Phys. Lett.* **2010**, *97*, 043305.
(63) Yuan, Y.; Zhang, J.; Sun, J.; Hu, J.; Zhang, T.; Duan, Y. Polymorphism and structural transition around 54 °C in regioregular poly(3-hexylthiophene) with high crystallinity as revealed by infrared spectroscopy. *Macromolecules* **2011**, *44*, 9341−9350.
(64) Nagamori, T.; Marumoto, K. Direct observation of hole accumulation in polymer solar cells during device operation using light-induced electron spin resonance. *Adv. Mater.* **2013**, *25*, 2362−2367.
(65) Wenger, O. S.; Leigh, B. S.; Villahermosa, R. M.; Gray, H. B.; Winkler, J. R. Electron tunneling through organic molecules in frozen glasses. *Science* **2005**, *307*, 99−102.
(66) Miller, J. R.; Beitz, J. V. Long-range transfer of positive charge between dopant molecules in a rigid glassy matrix. *J. Chem. Phys.* **1981**, *74*, 6746−6756.
(67) Lewis, F. D.; Letsinger, R. L.; Wasielewski, M. R. Dynamics of photoinduced charge transfer and hole transport in synthetic DNA hairpins. *Acc. Chem. Res.* **2001**, *34*, 159−170.
(68) Lewis, F. D.; Kalgutkar, R. S.; Wu, Y. S.; Liu, X. Y.; Liu, J. Q.; Hayes, R. T.; Miller, S. E.; Wasielewski, M. R. Driving force dependence of electron transfer dynamics in synthetic DNA hairpins. *J. Am. Chem. Soc.* **2000**, *122*, 12346−12351.
(69) Kobori, Y.; Yago, T.; Akiyama, K.; Tero-Kubota, S.; Sato, H.; Hirata, F.; Norris, J. R. Superexchange electron tunneling mediated by solvent molecules: Pulsed electron paramagnetic resonance study on electronic coupling in solvent-separated radical ion pairs. *J. Phys. Chem. B* **2004**, *108*, 10226−10240.
(70) Voityuk, A. A.; Rosch, N.; Bixon, M.; Jortner, J. Electronic coupling for charge transfer and transport in DNA. *J. Phys. Chem. B* **2000**, *104*, 9740−9745.
(71) Lan, Y.-K.; Huang, C.-I. A theoretical study of the charge transfer behavior of the highly regioregular poly-3-hexylthiophene in the ordered state. *J. Phys. Chem. B* **2008**, *112*, 14857−14862.
(72) Guo, J. M.; Ohkita, H.; Yokoya, S.; Benten, H.; Ito, S. Bimodal polarons and hole transport in poly(3-hexylthiophene):fullerene blend films. *J. Am. Chem. Soc.* **2010**, *132*, 9631−9637.
(73) Kobori, Y.; Fuki, M. Protein−ligand structure and electronic coupling of photoinduced charge-separated state: 9,10-Anthraquinone-1-sulfonate bound to human serum albumin. *J. Am. Chem. Soc.* **2011**, *133*, 16770−16773.